Weierstraß-Institut
für Angewandte Analysis und Stochastik

im Forschungsverbund Berlin e.V.

Preprint ISSN 0946 – 8633

Thin film dynamics on vertically rotating disks

K. Afanasiev [1], A. Münch [2], B. Wagner [1]

submitted: December 12, 2005

[1] Weierstrass Institute for Applied Analysis and Stochastics
Mohrenstrasse 39
10117 Berlin, Germany
E-Mail: afanasie@wias-berlin.de, wagnerb@wias-berlin.de

[2] Institute of Mathematics
Humboldt University
10099 Berlin, Germany
E-Mail: muench@mathematik.hu-berlin.de

No. 1074

Berlin 2005

1991 *Mathematics Subject Classification.* 76A20, 76D27, 65M60, 41A60.

Key words and phrases. Lubrication theory, matched asymptotic expansions, FEM, rotating flow, free boundary flow.

Edited by
Weierstraß-Institut für Angewandte Analysis und Stochastik (WIAS)
Mohrenstraße 39
D — 10117 Berlin
Germany

Fax: + 49 30 2044975
E-Mail: preprint@wias-berlin.de
World Wide Web: http://www.wias-berlin.de/

Abstract

The axisymmetric flow of a thin liquid film subject to surface tension, gravity and centrifugal forces is considered for the problem of a vertically rotating disk that is partially immersed in a liquid bath. This problem constitutes a generalization of the classic Landau-Levich drag-out problem to axisymmetric flow. A generalized lubrication model that includes the meniscus region connecting the thin film to the bath is derived. The resulting nonlinear fourth-order partial differential equation is solved numerically using a finite element scheme. For a range of parameters steady states are found. While the solutions for the height profile of the film near the drag-out region show excellent agreement with the asymptotic solutions to the corresponding classic Landau-Levich problem, they show novel patterns away from the meniscus region. The implications for possible industrial applications are discussed.

1 Introduction

The many industrial applications of rotating thin film flows have spurred numerous theoretical and experimental studies in the past. Starting with the work by Emslie et al. [5], various aspects of surface tension driven flow, including non-Newtonian effects [6], evaporation [16], Coriolis force [13], influencing the morphology and stability of the film, have since been investigated. As with these studies most of them dealt with a configuration where the fluid layer is moving on a horizontally rotating disk. Making use of the large scale separation between the small thickness of the film and the length scale of the evolving patterns, thin film models where used to obtain dimension-reduced models of the three-dimensional free boundary problems.

Far fewer studies are being found for the situation of a disk rotating about a horizontal axis and partially immersed in a bath of liquid thereby dragging out a thin film onto the disk. This problem involves the meniscus region, that connects

the film to the bath. As a consequence the scale separation in this region is not large anymore and hence the lubrication approximation is not valid there. However, the meniscus plays the crucial role of fixing the height of the drawn out liquid film and therefore the meniscus region that connects to the liquid bath must be accounted for. In a far simpler setting the free boundary problem of falling and rising thin film flows on vertical and inclined planes has been investigated as early as the pioneering work by Landau and Levich [11]. Their work lead to the prediction of the height and shape of the thin film emerging out of the meniscus. The results were improved by Wilson [19] and for the case of a Marangoni-driven rising film by Münch [12], using systematic asymptotic analysis in the limit of small capillary numbers. Their analyis was applied by Christodoulo et al. [2] in applications connected to flow control of rotating oil disk skimmers. Their study did not extend further into the flow field that governs the thin film region on the remainder of the disk. Up to now no complete model for the vertically rotating disk, including its numerical solution has appeared. This will be the topic of this paper.

While the solution to this problem will be of interest to problems such as the oil disk skimmer, the main application we have in mind is with respect to the fluid dynamical aspects in connection with the synthesis of Polyethylenterephthalat(PET), which is a commodity product with a wide range of applications, ranging from production of technical yarns to plastic bottles, see [1, 10, 17]. The synthesis of PET essentially proceeds in two reaction steps. The first one is an esterification reaction that produces a prepolymer. The second reaction step, which is subject of this study, is polycondensation within the melt phase. Here, all the important reactions are reversible balance reactions. In order to ensure high output rates, the low molecular weight by-products, such as Ethylenglykol (EG), have to be removed from the liquid reactants as efficiently as possible. Since the transport of EG within the liquid occurs predominantly by diffusion, which is a rather slow process, high removal rates can be achieved if the lengths across which EG has to diffuse is short, i.e. the liquid is spread out into thin films over a large area. PET is therefore produced in polycondensation reactors that typically consist of a horizontal cylinder which is partially filled with polymer melt and contains disks (perforated rings or nets) rotating about the horizontal axis of the cylinder, thus picking up and spreading the melt in form of a thin film over a large area of the disks. The fluid dynamical aspects play therefore an important role in the production of PET. One of the important challenge in this

application is the design that maximizes the active surface and the control of the resulting fluid dynamical problem. We consider here the spreading of a thin film on a single circular disk rotating about a horizontal axis and partially immersed in the reservoir with the liquid, see figure 1.

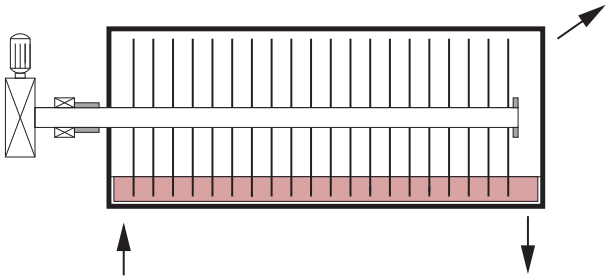

Figure 1: Cross section of a typical PET-reactor. Rotating disks are slightly immersed in a liquid bath.

In section 2 we set up the corresponding three-dimensional free boundary problem. A full three-dimensional analysis of such flows represents a very time consuming task, analytically and numerically. To be able to perform systematic parameter studies we therefore exploit the large separation of scales to obtain a dimension-reduced lubrication model. This model will then be extended to match to the flow field in the meniscus region. For the resulting model we develop in section 3 a weak formulation and a corresponding finite element discretization for the full dynamical problem. In section 4 we solve for a range of parameters the emerging steady state solutions. Their shapes near the meniscus region are then compared to the asymptotic solution of the corresponding drag-out problem, for which we find excellent agreement. Finally, we discuss the novel patterns for the film profile we find away from the meniscus region and discuss the possible implications on the PET synthesis.

2 Formulation

2.1 Governing Equations

We consider the isothermal flow of an incompressible, viscous liquid on a vertical disk rotating in the vertical plane and partially immersed in the liquid. We assume that the disk of radius R rotates with the angular velocity Ω about a horizontal axis, which has distance a to the bath, see figure 2.

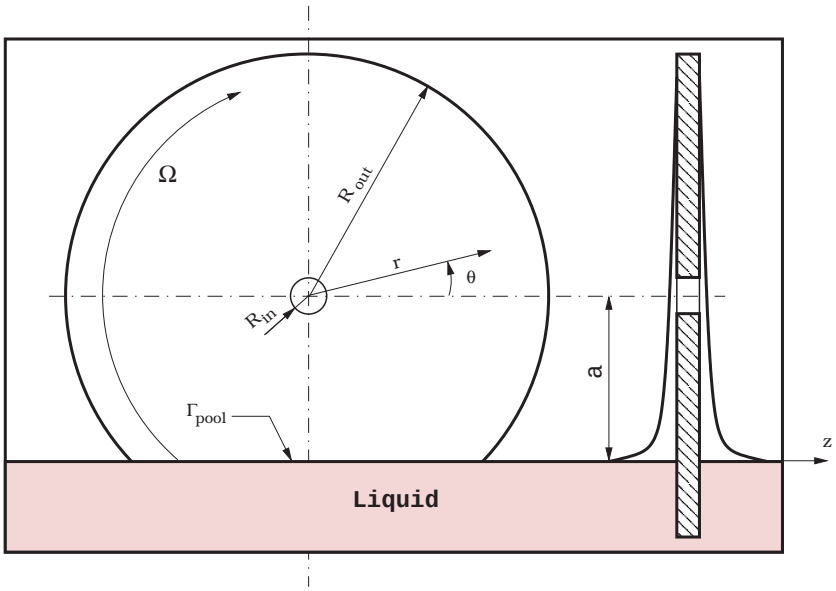

Figure 2: Configuration of a single disk within a PET-reactor

To formulate the problem, we introduce cylindrical polar coordinates (r, θ, z) in the laboratory frame of reference. We let the liquid velocity vector have components (u, v, w) and let ω denote the angular velocity vector with components $(0, 0, \Omega)$. The momentum balance equations can be expressed as

$$\rho\left[u_t + uu_r + \frac{v}{r}u_\theta - \frac{v^2}{r} + wu_z\right] = -p_r + \mu\left[\triangle u - \frac{2v_\theta}{r^2} - \frac{u}{r^2}\right] - \rho g \sin\theta \quad (2.1a)$$

$$\rho\left[v_t + uv_r + \frac{v}{r}v_\theta + \frac{uv}{r} + wv_z\right] = -\frac{p_\theta}{r} + \mu\left[\triangle v + \frac{2u_\theta}{r^2} - \frac{v}{r^2}\right] - \rho g \cos\theta \quad (2.1b)$$

$$\rho\left[w_t + uw_r + \frac{v}{r}w_\theta + ww_z\right] = -p_z + \mu \triangle w \quad (2.1c)$$

where

$$\triangle f = \frac{1}{r}(rf_r)_r + \frac{f_{\theta\theta}}{r^2} + f_{zz}. \quad (2.2)$$

We let ρ, μ and p denote the density, dynamic shear viscosity and the pressure of the liquid, respectively. The external force here is gravity and g denotes the gravitational constant.

The continuity equation is

$$\frac{1}{r}(ru)_r + \frac{1}{r}v_\theta + w_z = 0. \tag{2.3}$$

For the boundary condition at the surface of the disk, i.e. $z = 0$, that rotates with the velocity Ω, we impose the no-slip condition for u and v and the impermeability condition for w. Hence, we have

$$u = 0, \qquad v = r\Omega, \qquad w = 0, \tag{2.4}$$

respectively.

At the free boundary $z = h(r, \theta, t)$ we require the normal stress condition

$$\mathbf{n}\,\Pi\,\mathbf{n} = 2\sigma\kappa, \tag{2.5}$$

the tangential stress conditions

$$\mathbf{n}\,\Pi\,\mathbf{t}_i = 0, \qquad \text{where} \quad i = 1, 2, \tag{2.6}$$

and the kinematic condition

$$h_t = w - u_{|h}h_r - \frac{1}{r}v_{|h}h_\theta, \tag{2.7}$$

which can also be written, upon using the continuity equation, as

$$h_t = -\frac{1}{r}\frac{\partial}{\partial r}\, r \int_0^h u\, dz - \frac{1}{r}\frac{\partial}{\partial \theta}\int_0^h v\, dz. \tag{2.8}$$

The normal and the tangential vectors in radial and angular direction are given by

$$\mathbf{n} = \frac{(-h_r, -h_\theta/r, 1)}{(1 + h_r^2 + h_\theta^2/r^2)^{1/2}}, \quad \mathbf{t}_1 = \frac{(1, 0, h_r)}{(1 + h_\theta^2/r^2)^{1/2}}, \quad \mathbf{t}_2 = \frac{(0, 1, h_\theta/r)}{(1 + h_\theta^2/r^2)^{1/2}}, \tag{2.9}$$

respectively. The stress tensor Π is symmetric and has the components

$$\begin{aligned} &\Pi_{rr} = -p + 2\mu\, u_r, && \Pi_{\theta\theta} = -p + 2\mu\left(\frac{v_\theta}{r} + \frac{u}{r}\right), && \Pi_{zz} = -p + 2\mu w_z, \\ &\Pi_{r\theta} = \mu\left(\frac{u_\theta}{r} + v_r - \frac{v}{r}\right), && \Pi_{\theta z} = \mu\left(v_z + \frac{w_\theta}{r}\right), && \Pi_{rz} = \mu\left(w_r + u_z\right). \end{aligned} \tag{2.10}$$

Finally, we assume surface tension to be constant and denote it by σ and the mean curvature is given by

$$\kappa = \frac{1}{2}\left(\frac{1}{r}\frac{\partial}{\partial r}\frac{rh_r}{(1+h_r^2+h_\theta^2/r^2)^{1/2}} + \frac{1}{r}\frac{\partial}{\partial \theta}\frac{h_\theta/r}{(1+h_r^2+h_\theta^2/r^2)^{1/2}}\right). \tag{2.11}$$

Using this in equations (2.5) and (2.6) we obtain the boundary conditions for the normal stress

$$\begin{aligned} -p + \frac{2\mu}{1+h_r^2+h_\theta^2/r^2}\Bigg[&\left(\frac{u_\theta}{r}+v_r-\frac{v}{r}\right)\frac{h_r h_\theta}{r} \\ &-(w_r+u_z)h_r - \left(v_z+\frac{w_\theta}{r}\right)\frac{h_\theta}{r} + u_r h_r^2 + (v_\theta+u)\frac{h_\theta^2}{r^3} + w_z\Bigg] \\ &= \sigma\left[\frac{1}{r}\frac{\partial}{\partial r}\frac{rh_r}{(1+h_r^2+h_\theta^2/r^2)^{1/2}} + \frac{1}{r}\frac{\partial}{\partial \theta}\frac{h_\theta/r}{(1+h_r^2+h_\theta^2/r^2)^{1/2}}\right], \end{aligned} \tag{2.12}$$

the tangential stress condition in radial direction

$$\begin{aligned} 2(w_z-u_r)h_r - \left(\frac{u_\theta}{r}+v_r-\frac{v}{r}\right)\frac{h_\theta}{r} \\ +(w_r+u_z)(1-h_r^2) - \left(v_z+\frac{w_\theta}{r}\right)\frac{h_r h_\theta}{r} = 0 \end{aligned} \tag{2.13}$$

and the tangential stress condition in angular direction

$$\begin{aligned} 2\left(w_z-\frac{v_\theta}{r}-\frac{u}{r}\right)\frac{h_\theta}{r} - \left(\frac{u_\theta}{r}+v_r-\frac{v}{r}\right)h_r \\ +\left(v_z+\frac{w_\theta}{r}\right)\left(1-\frac{h_\theta^2}{r^2}\right) - (w_r+u_z)\frac{h_r h_\theta}{r} = 0. \end{aligned} \tag{2.14}$$

2.2 Lubrication approximation

The solution of the above three dimensional free boundary problem represents, analytically and numerically an enormously complex and time consuming task. The key idea that we make use of here in order to obtain a mathematically and numerically tractable problem, is the exploitation of the scale separation in most parts of this flow problem.

We begin by introducing dimensionsless variables and set

$$\begin{aligned} &r = L\bar{r}, \quad \theta = \bar{\theta}, \quad z = H\bar{z}, \\ &u = U\bar{u}, \quad v = U\bar{v}, \quad w = W\bar{w}, \\ &p = P\bar{p}, \quad t = T\bar{t}. \end{aligned} \tag{2.15}$$

The characteristic velocity U is set by the velocity of the rotating disk. For given radius R of the disk we let

$$U = R\Omega. \tag{2.16}$$

We determine the scale for the characteristic height H by balancing the dominant viscous term with gravitational term in the u-momentum equation, which yields

$$H = \sqrt{\frac{\mu U}{\rho g}}. \tag{2.17}$$

Furthermore, we require that the pressure must also balance the dominant viscous term, so that

$$P = \frac{\mu U L}{H^2} \tag{2.18}$$

and that surface tension is important, so that from the normal stress boundary condition we find

$$P = \frac{\sigma H}{L^2}. \tag{2.19}$$

This yields the scale for L as

$$L = \frac{H}{\left(\frac{\mu U}{\sigma}\right)^{1/3}} \tag{2.20}$$

and the time scale is fixed by $T = L/U$.

We assume that the liquid film is very thin and that the velocity in the direction normal to the disk is much smaller than along the disk. We let

$$\varepsilon = \frac{H}{L} \ll 1 \tag{2.21}$$

be a small parameter and $W = \varepsilon U$. Note that this also means that the capillary number Ca is small,

$$\mathrm{Ca}^{1/3} = \left(\frac{\mu U}{\sigma}\right)^{1/3} = \frac{H}{L} \ll 1. \tag{2.22}$$

With these scales the non-dimensional equations are

$$\begin{aligned}
\varepsilon^2\mathrm{Re}\left[u_t+uu_r+\frac{v}{r}u_\theta-\frac{v^2}{r}+wu_z\right] &= -p_r+u_{zz}-\sin\theta \qquad (2.23a)\\
&\quad +\varepsilon^2\left[\frac{(ru_r)_r}{r}+\frac{u_{\theta\theta}}{r^2}-\frac{2v_\theta}{r^2}-\frac{u}{r^2}\right],\\
\varepsilon^2\mathrm{Re}\left[v_t+uv_r+\frac{v}{r}v_\theta+\frac{uv}{r}+wv_z\right] &= -\frac{p_\theta}{r}+v_{zz}-\cos\theta \qquad (2.23b)\\
&\quad +\varepsilon^2\left[\frac{(rv_r)_r}{r}+\frac{v_{\theta\theta}}{r^2}+\frac{2u_\theta}{r^2}-\frac{v}{r^2}\right],\\
\varepsilon^4\mathrm{Re}\left[w_t+uw_r+\frac{v}{r}w_\theta+ww_z\right] &= -p_z+\varepsilon^2w_{zz} \qquad (2.23c)\\
&\quad +\varepsilon^4\left[\frac{(rw_r)_r}{r}+\frac{w_{\theta\theta}}{r^2}\right],
\end{aligned}$$

where the Reynolds number is $\mathrm{Re}=\rho UL/\mu$ and we have dropped the '$-$'s.

The boundary conditions at the disk, $z=0$ are

$$u=0, \qquad v=\alpha r, \qquad w=0, \qquad (2.24)$$

where $\alpha=L/R$.

The boundary conditions at the free liquid surface $z=h(r,\theta,t)$ are the conditions for normal and tangential stresses

$$\begin{aligned}
-p+\frac{2\varepsilon^2}{1+\varepsilon^2h_r^2+\varepsilon^2h_\theta^2/r^2}&\left[\varepsilon^2\left(\frac{u_\theta}{r}+v_r-\frac{v}{r}\right)\frac{h_rh_\theta}{r}\right.\\
&\left.-(\varepsilon^2w_r+u_z)h_r-\left(v_z+\varepsilon^2\frac{w_\theta}{r}\right)\frac{h_\theta}{r}+\varepsilon^2u_rh_r^2+\varepsilon^2(v_\theta+u)\frac{h_\theta^2}{r^3}+w_z\right] \qquad (2.25)\\
&=\left[\frac{1}{r}\frac{\partial}{\partial r}\frac{rh_r}{(1+\varepsilon^2h_r^2+\varepsilon^2h_\theta^2/r^2)^{1/2}}+\frac{1}{r}\frac{\partial}{\partial\theta}\frac{h_\theta/r}{(1+\varepsilon^2h_r^2+\varepsilon^2h_\theta^2/r^2)^{1/2}}\right],
\end{aligned}$$

$$\begin{aligned}
2\varepsilon^2(w_z-u_r)h_r-\varepsilon^2\left(\frac{u_\theta}{r}+v_r-\frac{v}{r}\right)\frac{h_\theta}{r} \qquad (2.26)\\
+(\varepsilon^2w_r+u_z)(1-\varepsilon^2h_r^2)-\varepsilon^2\left(v_z+\varepsilon^2\frac{w_\theta}{r}\right)\frac{h_rh_\theta}{r}=0,
\end{aligned}$$

$$\begin{aligned}
2\varepsilon^2\left(w_z-\frac{v_\theta}{r}-\frac{u}{r}\right)\frac{h_\theta}{r}-\varepsilon^2\left(\frac{u_\theta}{r}+v_r-\frac{v}{r}\right)h_r \qquad (2.27)\\
+\left(v_z+\varepsilon^2\frac{w_\theta}{r}\right)\left(1-\varepsilon^2\frac{h_\theta^2}{r^2}\right)-\varepsilon^2\left(\varepsilon^2w_r+u_z\right)\frac{h_rh_\theta}{r}=0,
\end{aligned}$$

and the kinematic boundary condition

$$\frac{\partial h}{\partial t} = -\frac{1}{r}\frac{\partial}{\partial r}\left(r\int_0^h u\,\mathrm{d}z\right) - \frac{1}{r}\frac{\partial}{\partial \theta}\left(\int_0^h v\,\mathrm{d}z\right). \tag{2.28}$$

2.3 Meniscus region

The scalings introduced so far are appropriate for the thin film region away from the liquid bath. This yields a leading order theory that retains the terms that are dominant for the film profile on the disk, where slopes are small. Near and in the meniscus, the film profile becomes (in fact infinitely) steep and a lubrication scaling is no longer appropriate. Rather, the profile is governed by the balance of gravity and surface tension forces, much as in a static meniscus, hence the appropriate length scales for all spatial coordinates is the capillary length scale $l_{\mathrm{cap}} = \sqrt{\sigma/(\rho g)}$.

This length scale can be easily expressed in terms of the lubrication length scales H and L times an appropriate power of ε, so that the new length scales (denoted by tildes) become

$$\tilde{H} = \varepsilon^{-3/2}H, \qquad \tilde{L} = \varepsilon^{-1/2}L. \tag{2.29}$$

The parallel velocity scale is unchanged and equal to $U = R\Omega$, while the normal is now U, too, instead of εU. The time scale

$$\tilde{T} = \frac{\tilde{L}}{U} = \varepsilon^{-1/2}T, \tag{2.30}$$

again is a result of the kinematic condition. The pressure scale is determined by surface tension, and we find

$$\tilde{P} = \sqrt{\sigma\rho g} = \varepsilon^{-1/2}P. \tag{2.31}$$

Hence, all variables can be transformed to meniscus scalings simply by rescaling with powers of ε, according to

$$\begin{aligned} r &= \varepsilon^{-1/2}\tilde{r}, \quad & z &= \varepsilon^{-3/2}\tilde{z}, \quad & h &= \varepsilon^{-3/2}\tilde{h}, \\ u &= \tilde{u}, & v &= \tilde{v}, & w &= \varepsilon^{-1}\tilde{w}, \\ t &= \varepsilon^{-1/2}\tilde{t}, & p &= \varepsilon^{-1/2}\tilde{p}. \end{aligned} \tag{2.32}$$

Inserting these scalings into (2.23a)–(2.28), yields the rescaled equations:

$$\begin{aligned}
\varepsilon^3\mathrm{Re}\left[u_t + uu_r + \frac{v}{r}u_\theta - \frac{v^2}{r} + wu_z\right] &= -p_r + \varepsilon^3 u_{zz} - \sin\theta \qquad (2.33a)\\
&\quad +\varepsilon^3\left[\frac{(ru_r)_r}{r} + \frac{u_{\theta\theta}}{r^2} - \frac{2v_\theta}{r^2} - \frac{u}{r^2}\right],\\
\varepsilon^3\mathrm{Re}\left[v_t + uv_r + \frac{v}{r}v_\theta + \frac{uv}{r} + wv_z\right] &= -\frac{p_\theta}{r} + \varepsilon^3 v_{zz} - \cos\theta \qquad (2.33b)\\
&\quad +\varepsilon^3\left[\frac{(rv_r)_r}{r} + \frac{v_{\theta\theta}}{r^2} + \frac{2u_\theta}{r^2} - \frac{v}{r^2}\right],\\
\varepsilon^4\mathrm{Re}\left[w_t + uw_r + \frac{v}{r}w_\theta + ww_z\right] &= -p_z + \varepsilon^3 w_{zz} \qquad (2.33c)\\
&\quad +\varepsilon^3\left[\frac{(rw_r)_r}{r} + \frac{w_{\theta\theta}}{r^2}\right],
\end{aligned}$$

where the Reynolds number is $\mathrm{Re} = \rho UL/\mu = \varepsilon^{1/2}\rho U\tilde{L}/\mu = \varepsilon^{1/2}\tilde{\mathrm{Re}}$ and where we have dropped the '˜'s.

The boundary conditions at the disk, $z = 0$ are

$$u = 0, \qquad v = \hat{\alpha}r, \qquad w = 0, \tag{2.34}$$

where $\hat{\alpha} = \ell_{cap}/R$.

The boundary conditions for normal and tangential stresses become at $z = h(r,\theta,t)$:

$$\begin{aligned}
-p + \frac{2\varepsilon^3}{1 + h_r^2 + h_\theta^2/r^2}&\left[\left(\frac{u_\theta}{r} + v_r - \frac{v}{r}\right)\frac{h_r h_\theta}{r}\right.\\
&\left.-(w_r + u_z)h_r - \left(v_z + \frac{w_\theta}{r}\right)\frac{h_\theta}{r} + u_r h_r^2 + (v_\theta + u)\frac{h_\theta^2}{r^3} + w_z\right] \qquad (2.35)\\
&= \left[\frac{1}{r}\frac{\partial}{\partial r}\frac{rh_r}{(1 + h_r^2 + h_\theta^2/r^2)^{1/2}} + \frac{1}{r}\frac{\partial}{\partial\theta}\frac{h_\theta/r}{(1 + h_r^2 + h_\theta^2/r^2)^{1/2}}\right],
\end{aligned}$$

$$\begin{aligned}
2(w_z - u_r)h_r - \left(\frac{u_\theta}{r} + v_r - \frac{v}{r}\right)\frac{h_\theta}{r} &\qquad (2.36)\\
+(w_r + u_z)(1 - h_r^2) - \left(v_z + \frac{w_\theta}{r}\right)\frac{h_r h_\theta}{r} &= 0,
\end{aligned}$$

$$\begin{aligned}
2\left(w_z - \frac{v_\theta}{r} - \frac{u}{r}\right)\frac{h_\theta}{r} - \left(\frac{u_\theta}{r} + v_r - \frac{v}{r}\right)h_r &\qquad (2.37)\\
+\left(v_z + \frac{w_\theta}{r}\right)\left(1 - \frac{h_\theta^2}{r^2}\right) - (w_r + u_z)\frac{h_r h_\theta}{r} &= 0.
\end{aligned}$$

We now retain all terms that appear to leading order either in the lubrication or the meniscus scalings. Note that, in the meniscus scalings, the velocity field decouples to leading order from the pressure field that determines the surface profile. Hence the dominant terms that govern h in these scalings consists of the pressure and gravity terms, and of surface tension, based on the full nonlinear expression for curvature. All these terms already appear also in the lubrication scaling, except for the nonlinear curvature. Hence our approximate model retains essentially the terms from a leading order lubrication theory and the nonlinear curvature term, i.e., in the bulk we have,

$$0 = -p_r + \varepsilon^3 u_{zz} - \sin\theta, \qquad 0 = -\frac{p_\theta}{r} + \varepsilon^3 v_{zz} - \cos\theta, \qquad 0 = -p_z. \tag{2.38}$$

Boundary conditions at $z = 0$ are given by (2.34), and at $z = h$:

$$-p = \left[\frac{1}{r}\frac{\partial}{\partial r}\frac{r h_r}{(1 + h_r^2 + h_\theta^2/r^2)^{1/2}} + \frac{1}{r}\frac{\partial}{\partial\theta}\frac{h_\theta/r}{(1 + h_r^2 + h_\theta^2/r^2)^{1/2}}\right], \quad u_z = 0, \qquad v_z = 0. \tag{2.39}$$

Integrating first $p_z = 0$ yields a solution that does not depend on z, and the parallel components for the velocity can easily be found to be

$$u = \varepsilon^{-3}(p_r - \sin\theta)(z^2/2 - hz), \qquad v = \varepsilon^{-3}(p_\theta/r - \cos\theta)(z^2/2 - hz) + \hat{\alpha} r. \tag{2.40}$$

We plug this into the mass conservation relation (2.8), which in meniscus variables is unchanged,

$$h_t = -\frac{1}{r}\frac{\partial}{\partial r} r \int_0^h u\, dz - \frac{1}{r}\frac{\partial}{\partial\theta}\int_0^h v\, dz,$$

and obtain, after rescaling time once more according to $t = \epsilon^{-3} t'$ (dropping the prime):

$$h_t = \frac{1}{r}\frac{\partial}{\partial r}\left[r\frac{h^3}{3}(p_r + \sin\theta)\right] + \frac{1}{r}\frac{\partial}{\partial\theta}\left[\frac{h^3}{3}(p_\theta/r + \cos\theta) - \hat{\Omega} r h\right], \tag{2.41}$$

where we have introduced $\hat{\Omega} = \mu\Omega/\sqrt{\rho g \sigma}$.

For the boundary conditions of equation (2.41) we require that the curvature approaches zero as the free surface approaches the reservoir Γ_{pool}, which is defined by the line $r = -a/\sin\theta$. Hence,

$$p(r, \theta, t) \to 0 \quad \text{as} \quad r \to -a/\sin\theta. \tag{2.42}$$

The height towards the reservoir is chosen large enough with respect to the height of the thin film until the resulting film profile has converged. We set

$$h \to 1 \quad \text{as} \quad r \to -a/\sin\theta. \tag{2.43}$$

Towards the inner ($r = R_{in}$) and outer ($r = R_{out}$) confinements of the disk we assume *natural* boundary conditions, i.e.

$$p_r + sin\theta = 0, \quad \text{as} \quad r \to R_{in}, R_{out}, \tag{2.44}$$

$$h_r = 0, \quad \text{as} \quad r \to R_{in}, R_{out}. \tag{2.45}$$

3 Numerical method

3.1 Differential formulation

The meniscus equations may be rewritten for simlicity as

$$r\,\frac{\partial h}{\partial t} = \frac{\partial Q^r}{\partial r} + \frac{\partial Q^\theta}{\partial \theta}, \tag{3.46}$$

$$-\frac{1}{2}\,r\,p = \frac{\partial q^r}{\partial r} + \frac{\partial q^\theta}{\partial \theta}, \tag{3.47}$$

where fluxes Q^r, q^r and Q^θ, q^θ in r and θ directions are defined, respectively:

$$Q^r = r\frac{h^3}{3}(p_r + \sin\theta), \qquad q^r = \frac{rh_r}{\sqrt{1 + h_r^2 + h_\theta^2/r^2}}, \tag{3.48}$$

$$Q^\theta = \frac{h^3}{3}(\frac{1}{r}p_\theta + \cos\theta) + r\Omega h, \quad q^\theta = \frac{h_\theta}{r\sqrt{1 + h_r^2 + h_\theta^2/r^2}}. \tag{3.49}$$

For the outlet boundary condition we take natural boundary condition, i.e. zero fluxes in the direction of a normal vector.

$$Q^r(r,\theta,t) = 0, \qquad r \to R_{out}, \tag{3.50}$$

$$q^r(r,\theta,t) = 0, \qquad r \to R_{out}. \tag{3.51}$$

Similarly, we choose for the conditions towards the origin natural boundary condition

$$Q^r(r,\theta,t) = 0, \qquad r \to R_{in}, \tag{3.52}$$

$$q^r(r,\theta,t) = 0, \qquad r \to R_{in}. \tag{3.53}$$

For the immersing boundary condition, where the meniscus connects to the liquid bath we let the curvature of the free surface vanish. Hence, we require the boundary conditions (2.42) and (2.43).

3.2 Weak formulation

The weak formulation of the equation systems (3.46, 3.47) under the boundary conditions (3.50)-(3.53) and (2.42, 2.43) can be derived by the multiplying (3.46) and (3.47) by a suitable test function ϕ, integrating over the domain Λ and evaluating of the boundary conditions. Then the weak formulation of the boundary value problem for (3.46,3.47) requires to seek $(h, p) \in H^1$, such that

$$\int_\Lambda r\frac{\partial h}{\partial t}\,\phi\,\mathrm{d}\Lambda = -\int_\Lambda \left(Q^r\frac{\partial \phi}{\partial r} + Q^\theta\frac{\partial \phi}{\partial \theta}\right)\,\mathrm{d}\Lambda + \int_\Gamma Q^r\,\phi\,n_r\,\mathrm{d}\Gamma\,, \tag{3.54}$$

$$\frac{1}{2}\int_\Lambda r\,p\,\phi\,\mathrm{d}\Lambda = \int_\Lambda \left(q^r\,\frac{\partial \phi}{\partial r} + q^\theta\frac{\partial \phi}{\partial \theta}\right)\,\mathrm{d}\Lambda - \int_\Gamma q^r\phi\,n_r\,\mathrm{d}\Gamma \tag{3.55}$$

for all functions $\phi \in V$. Respecting the boundary conditions $p_r = 0,\ h_r = 0$, the following integral equations

$$\int_\Lambda r\frac{\partial h}{\partial t}\,\phi\,\mathrm{d}\Lambda = -\int_\Lambda \left(Q^r\frac{\partial \phi}{\partial r} + Q^\theta\frac{\partial \phi}{\partial \theta}\right)\,\mathrm{d}\Lambda + \int_\Gamma \left(\frac{rh^3}{3}sin\theta\,\phi\right)\,\mathrm{d}\Gamma\,, \tag{3.56}$$

$$\frac{1}{2}\int_\Lambda r\,p\,\phi\,\mathrm{d}\Lambda = \int_\Lambda \left(q^r\,\frac{\partial \phi}{\partial r} + q^\theta\frac{\partial \phi}{\partial \theta}\right)\,\mathrm{d}\Lambda \tag{3.57}$$

will now be discretised.

3.3 Finite element scheme

For the discretisation of the problem we devide the domain Λ in non-overlapping triangular elements Λ_e and replace $H^1(\Lambda)$ and $V(\Lambda)$ by finite dimensional subspaces S and V^h, respectively. We also choose $\phi = \phi_i,\ i = 1, 2, \ldots, N$ with N denoting the number of nodes in the element Λ_e and let

$$h_e(r, \theta, t) = \sum_{i=1,N} h_i(t)\phi_i(r, \theta)\,, \tag{3.58}$$

$$p_e(r, \theta, t) = \sum_{i=1,N} p_i(t)\phi_i(r, \theta) \tag{3.59}$$

be the functions that approximate h and p on this element, respectively. The domain integrals can now be replaced by the sum of integrals taken separatly over the elements of triangulation.

Let the time interval $[0,T]$ be subdivided into intervals with the time step τ, $t_n = t_{n-1} + \tau,\ n = 1, 2, \ldots, N_T$ and denote

$$h^n = \begin{pmatrix} h_1(t^n) \\ h_2(t^n) \\ \vdots \\ h_N(t^n) \end{pmatrix}, \qquad p^n = \begin{pmatrix} p_1(t^n) \\ p_2(t^n) \\ \vdots \\ p_N(t^n) \end{pmatrix}.$$

By substitution of equations (3.58, 3.59) into the weak formulation and its implicit backward Euler discretisation, expressions (3.56, 3.57) can be written in matrix notation as the following finite nonlinear system

$$Lh^{n+1} + \tau \left[C^r g_1^h(h^{n+1}, p^{n+1}) + C^\theta g_2^h(h^{n+1}, p^{n+1}) + s(h^{n+1}) \right] = Lh^n, \tag{3.60}$$

$$Lp^{n+1} = 2 \left[C^r g_1^p(h^{n+1}) + C^\theta g_2^p(h^{n+1}) \right] \tag{3.61}$$

where matrices and vectors are defined by

$$L_{ij} = \int_{\Lambda_e} r\, \phi_i\, \phi_j \, \mathrm{d}\Lambda\,, \tag{3.62}$$

$$C^r_{ij} = \int_{\Lambda_e} \frac{\partial \phi_i}{\partial r}\, \phi_j \, \mathrm{d}\Lambda\,, \tag{3.63}$$

$$C^\theta_{ij} = \int_{\Lambda_e} \frac{\partial \phi_i}{\partial \theta}\, \phi_j \, \mathrm{d}\Lambda\,, \tag{3.64}$$

$$M_{ij} = \int_{\Lambda_e} \phi_i\, \phi_j \, \mathrm{d}\Lambda\,, \tag{3.65}$$

$$g_1^h = \frac{rw}{3} \left(q_r^p + sin\theta \right)\,, \tag{3.66}$$

$$g_2^h = \frac{w}{3} \left(\frac{q_\theta^p}{r} + cos\theta + r\, \Lambda\, h \right)\,, \tag{3.67}$$

$$g_1^p = \frac{r q_r^h}{(1 + (q_r^h)^2 + (q_\theta^h)^2/r^2)^{\frac{1}{2}}}\,, \tag{3.68}$$

$$g_2^p = \frac{q_\theta^h}{r^2 (1 + (q_r^h)^2 + (q_\theta^h)^2/r^2)^{\frac{1}{2}}}\,, \tag{3.69}$$

$$
\begin{aligned}
w &= M^{-1}a\,, && (3.70)\\
a_i &= \sum_{m,l,j} h_m\, h_l\, h_j \int_{\Lambda} \phi_m\, \phi_l\, \phi_j\, \phi_i\, \mathrm{d}\Lambda\,, && (3.71)\\
Y^r &= M^{-1}(C^r)^T, \qquad Y^\theta = M^{-1}(C^\theta)^T\,, && (3.72)\\
q_r^h &= Y^r\, h, \qquad q_\theta^h = Y^\theta\, h\,, && (3.73)\\
q_r^p &= Y^r\, p, \qquad q_\theta^p = Y^\theta\, p\,, && (3.74)\\
s_i &= \begin{cases} 0, & \Gamma_e := \Lambda_e \bigcap \Gamma = 0\,, \\ \int\limits_{\Gamma_e} \left(\frac{h_i^3}{3}\; r\; sin\theta\right)\, \mathrm{d}\Gamma\,, & \Gamma_e \neq 0\,. \end{cases} && (3.75)
\end{aligned}
$$

Evaluation of matrix and vector coefficients The various element matricies and vectors expressed by the equations above are spatial integrals of the various interpolation functions and their derivatives. These integrals can be evaluated analytically. The remaining ones are obtained using numerical quadrature procedure. Matrix and vector coefficients for triangular elements are evaluated using a seven-point quadrature scheme for quadratic triangles.

Triangulation We use the six node quadratic triangular elements as shown in Figure 3 and following basic functions written in the so called natural coordinates $L_i, i = 1, 2, 3$ based on area ratios (see in [9]). The grids were generated by using

$$
\begin{aligned}
\phi_1 &= L_1(2L_1 - 1)\\
\phi_2 &= L_2(2L_2 - 1)\\
\phi_2 &= L_3(2L_3 - 1)\\
\phi_4 &= 4L_1L_2\\
\phi_5 &= 4L_2L_3\\
\phi_6 &= 4L_3L_1
\end{aligned}
$$

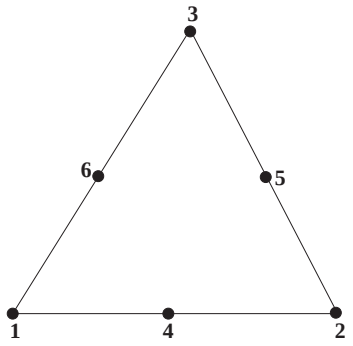

Figure 3: Basic functions for a six node quadratic triangular element

the automatic mesh generator [15] based upon the Delaunay refinement algorithm.

Assembling the global equation system The contributions of the element coefficient matrices and vectors (3.62)-(3.75) are added by the common global

node for the assembling of the global nonlinear equation system similar to [7]. The global equation system can be written in the form

$$R(U) = F, \tag{3.76}$$

where U is constructed from the vectors h^{n+1} and p^{n+1} in all grid nodes.

Time stepping The time stepping algorithm is customarily implemented with a Newton-Raphson equilibrium iteration loop. In the each time step the following nonlinear problem must be solved

$$G(U) := R(U) - F = 0. \tag{3.77}$$

The linearized equation can be written on the basis of the Taylor expansion

$$G(U_{i+1}) = G(U_i) + \underbrace{\left.\frac{\partial G}{\partial U}\right|_{U=U_i}}_{K(U_i)} \triangle U_{i+1}.$$

At each step of Newton's method, some direct or iterative method must be used to solve the large linear algebra problem produced by the two-dimensional linearized operator

$$K(U_i)\,\triangle U_{i+1} = -G(U_i) \tag{3.78}$$

$$\text{with} \qquad U_{i+1} = U_i + \triangle U_{i+1}\,. \tag{3.79}$$

Here, we find it convenient to use the non-symmetric multi-frontal method for large sparse linear systems from the packet UMFPACK [4].

4 Steady states

4.1 Numerical results

We consider here a disk rotating about the horizontal axis with a constant angular speed Ω and being, for the rest of this study, half-immersed in the liquid bath. The triangulation of the computational domain was made in cylindrical coordinates r, θ. The finite element mesh, used here, consists of 9533 triangular elements and 19522 nodes. The mesh, shown in Fig. 4, was extra refined on the boundary

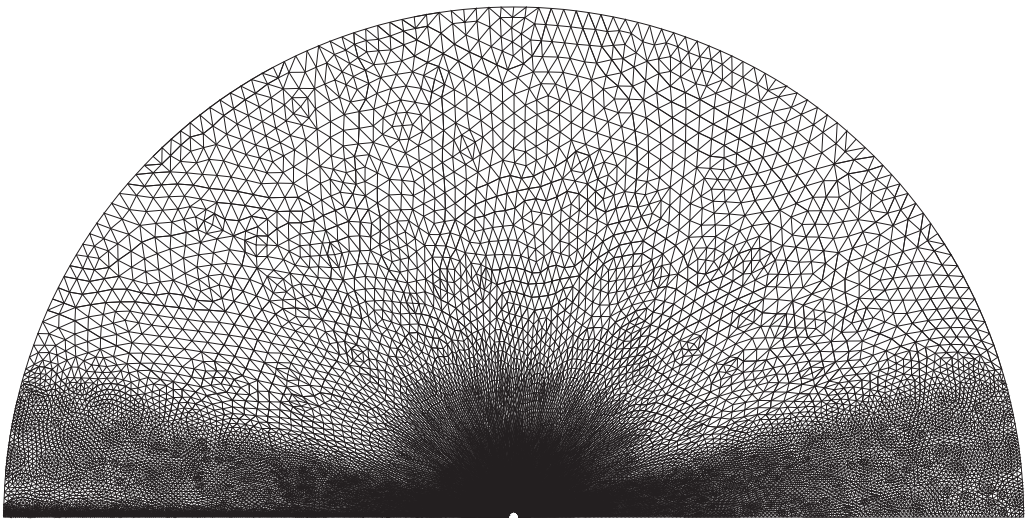

Figure 4: Finite Element mesh with 19522 nodes.

Γ_{pool} to resolve the meniskus region. The steady state was obtained via time integration with a adaptiv time step of equations (3.46, 3.47) with a inertial term and following newton iterations of their without inertial term. As stopping criterion for the newton iterations a general threshold for the residuum $||G(U)|| < 10^{-13}$ is applied. The values of the parameters are chosen to model a glycerin film:

$$\begin{aligned} \mu &= 1 \quad \text{Pa s}, \quad \rho = 1000 \quad \text{kg/m}^3, \quad \sigma = 72.7e-3 \quad \text{N/m}, \\ R &= 2.723e-2 \quad \text{m}, \quad U = 7.917e-4 \quad \text{m/s}, \quad g = 9.81 \quad \text{m/s}^2. \end{aligned} \tag{4.80}$$

The initial state has partially constant profile on the top of the disk and partially parabolic one around the bath, shown in the Figure 5.

For this U and R we find the angular velocity $\Omega = U/R = 0.02908$ s^{-1} = 0.277 r.p.m. , where the last equality is obtained by multiplying with $60/2\pi$. For these values we obtain $\hat{\Omega} = 1.089e-3$, the capillary number Ca = 0.01089, and length scales $\tilde{H} = \tilde{L} = l_{\text{cap}} = (\sigma/\rho g)^{1/2} = 2.723e-3$ m. The dimensionless radius of the disk is therefore 10.

In the following, we will also consider angular velocities of 1.0, 2.0, 3.0 r.p.m, while keeping the other dimensional parameters and disk radius fixed. This does not change the length scales nor the dimensionless radius of the disk, but it changes

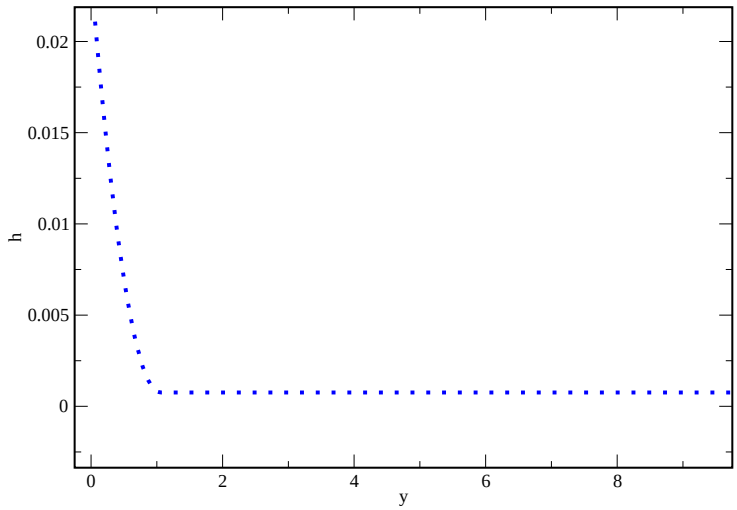

Figure 5: Initial state.

U, the capillary number and $\hat{\Omega}$:

$$\Omega = 1.0 \quad \text{r.p.m.}: \quad U = 0.2851e-2 \quad \text{m/s}, \quad \text{Ca} = 0.03922, \quad \hat{\Omega} = 3.922e-3,$$
$$\Omega = 2.0 \quad \text{r.p.m.}: \quad U = 0.5703e-2 \quad \text{m/s}, \quad \text{Ca} = 0.07845, \quad \hat{\Omega} = 7.843e-3,$$
$$\Omega = 3.0 \quad \text{r.p.m.}: \quad U = 0.8555e-2 \quad \text{m/s}, \quad \text{Ca} = 0.1177, \quad \hat{\Omega} = 1.176e-2,$$

Figures 6, 7 illustrate the steady states obtained for the fluid with the physical properties of glycerin and a range of rotation velocities of the disk $\Omega = 0.277, 1.0, 2.0, 3.0$ r.p.m., respectively.

One observes for all values of Ω of the steady solutions a region of liquid drag out with a meniscus profile and a region with a capillary wave on the opposite side of the axis. Such an oscillation of the height is typically found for the reverse Landau-Levich problem when a liquid thin film is falling into a liquid bath, see for example [3, 8, 18, 20]. It can be seen more clearly when comparing the cross sections of the liquid profiles at constant radii. In figure 8 we compare for the radius $r = 9$ the cross section for $\Omega = 0.277, 1.0, 2.0, 3.0$ r.p.m. (Note, that here as further below, values such as for r without an explicit dimensions are in fact dimensionless). The figure also shows that the the average liquid height increases when Ω increases.

These results are qualitatively in accordance with the Landau-Levich problem for

the drag-out and falling film cases. We will further investigate the quantitative comparison, which we expect to yield good results close to the meniscus region.

4.2 Asymptotic estimate of the film thickness

We now derive an asymptotic approximation of the film thickness using a one dimensional approximation based on the results of Landau, Levich [11] and Wilson [19] for the planar-symmetric case.

For our comparisons we focus on the case where the disk is half immersed, i.e. $a = 0$. Then, if we only retain the axial components in the stationary form of (2.41), and after substituting $r\theta \mapsto y$, $rd\theta \mapsto dy$ we obtain the equation

$$\frac{d}{dy}\left[\frac{h^3}{3}(p_y + 1) - \hat{\Omega} r h\right] = 0, \tag{4.81}$$

with

$$p = -\frac{d}{dy}\frac{h_y}{(1 + h_y^2)^{1/2}} \ . \tag{4.82}$$

Boundary conditions are

$$\lim_{y\to\infty} h = h_\infty, \qquad \lim_{y\to 0} h = \infty, \quad \lim_{y\to 0} p = 0. \tag{4.83}$$

Integrating (4.81), (4.82) once and using the boundary conditions (4.83) yields

$$h^3 \frac{d^2}{dy^2}\frac{h_y}{(1 + h_y^2)^{1/2}} = -3r\hat{\Omega}(h - h_\infty) + (h^3 - h_\infty^3). \tag{4.84}$$

We rescale this equation to bring it into the form

$$h = (r\hat{\Omega})^{1/2}\bar{h}, \quad h_\infty = (r\hat{\Omega})^{1/2}\bar{h}_\infty, \quad y = (r\hat{\Omega})^{1/6}\bar{y}, \tag{4.85}$$

to get

$$\bar{h}^3 \frac{d^2}{d\bar{y}^2}\frac{\bar{h}_{\bar{y}}}{\left(1 + (r\hat{\Omega})^{2/3}\bar{h}_{\bar{y}}^2\right)^{1/2}} = -3(\bar{h} - \bar{h}_\infty) + (\bar{h}^3 - \bar{h}_\infty^3). \tag{4.86}$$

For this equation, Wilson's formula [19] gives the asymptotic approximation for the film thickness

$$\bar{h}_\infty = 0.94581\,(r\hat{\Omega})^{1/6},$$

i.e. from (4.85),

$$h_\infty = 0.94581\,(r\hat{\Omega})^{2/3}. \tag{4.87}$$

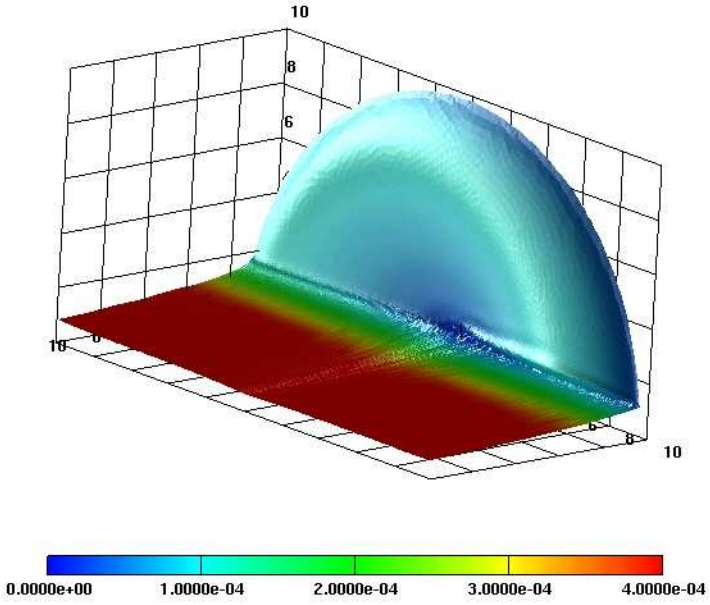

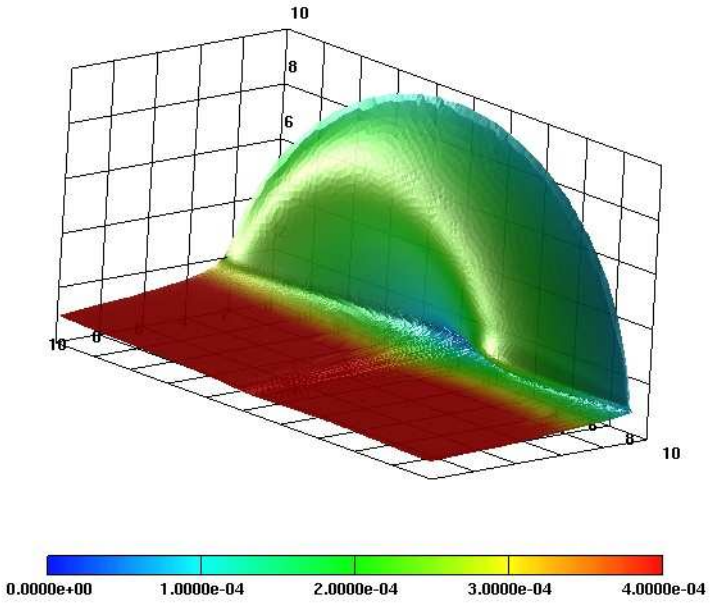

Figure 6: Steady solutions for glycerin at $\Omega = 0.277, 1.0,$ r.p.m.

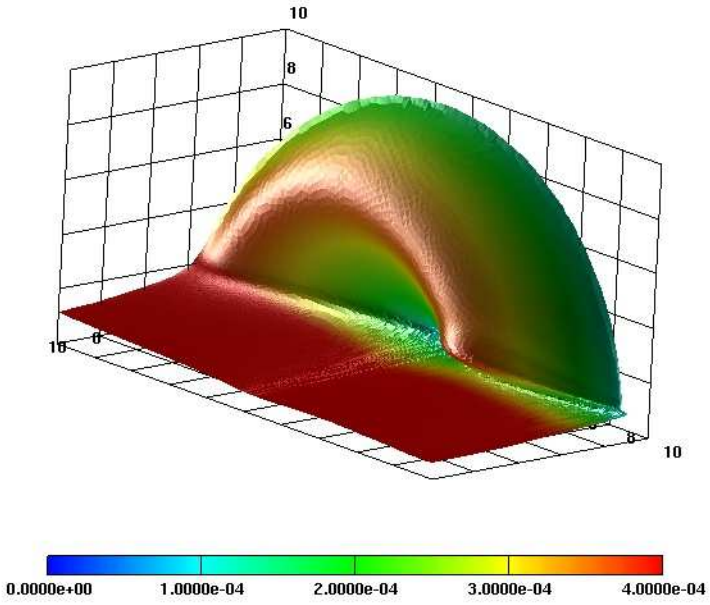

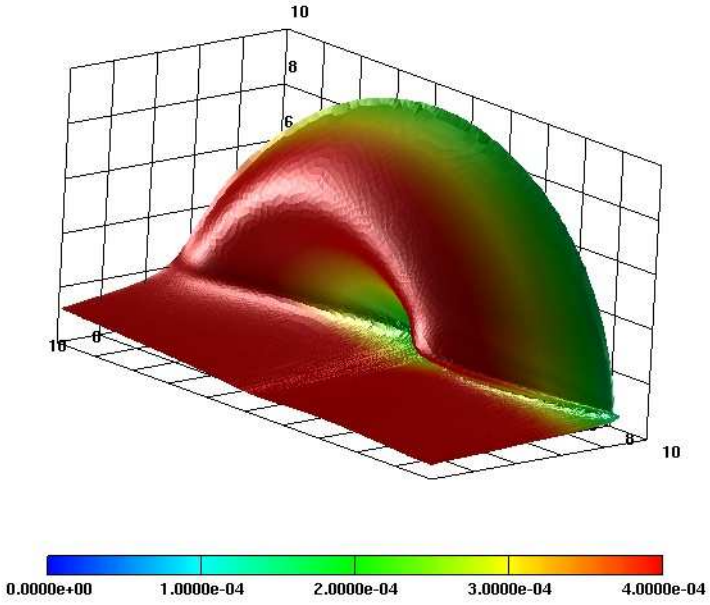

Figure 7: Steady solutions for glycerin at $\Omega = 2.0, 3.0$ r.p.m.

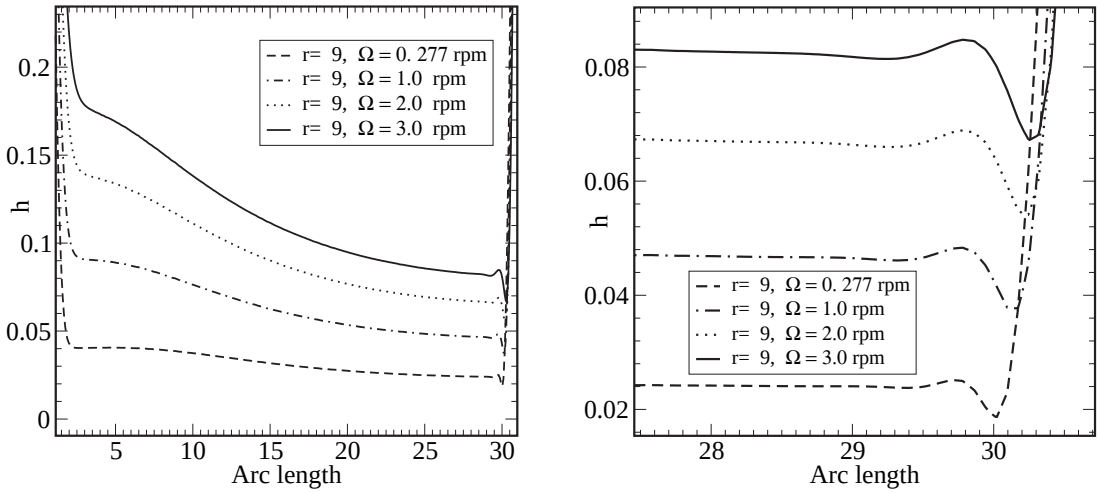

Figure 8: Comparisons of the profiles of the cross sections for the film profile for radius $r = 9$. On the right hand side where the film is pulled into the bath a capillary wave is formed. This region is enlarged on the right figure. Note, "Arc length" denotes $r\theta$.

Figure 9 shows h_∞ as a function of $r\hat{\Omega}$. Good agreement of the one-dimensional numerical results with the corresponding higher order asymptotic formula is achieved for small values of $r\hat{\Omega}$.

4.3 Comparison with the Landau-Levich problem

The meniscus profile $h(y)$ in figure 10 is now computed for the values given in (4.80). Recall that $\hat{\Omega} = 1.089e - 3$. At $r = 9$, we have $r\hat{\Omega} = 0.009801$, hence, from (4.87), $h_\infty = 0.0433$.

We now compare the meniscus profile computed with (4.86) for the Landau-Levich problem with the steady state solution to our problem for the rotating disk. For this we take results for the cross section along constant radii. In figure 10 we performed the comparison for the cross section for the height profile at radius $r = 9$, for $0 \leq \theta \leq 180$, i.e. from the point where the film is dragged out to the point where it reenters the liquid bath for the case, where $\Omega = 0.277$ r.p.m. We see that there is excellent quantitative agreement in the vicinity of the meniscus region as it enters the thin film region.

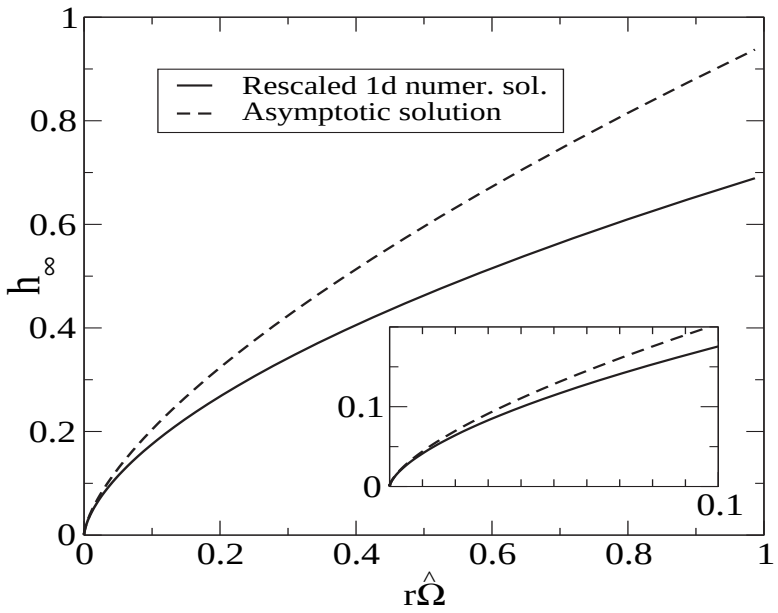

Figure 9: Comparison of numerical results for the one-dimensional problem (4.84) with the asymptotic formula for h_∞ versus $r\hat{\Omega}$, (4.87).

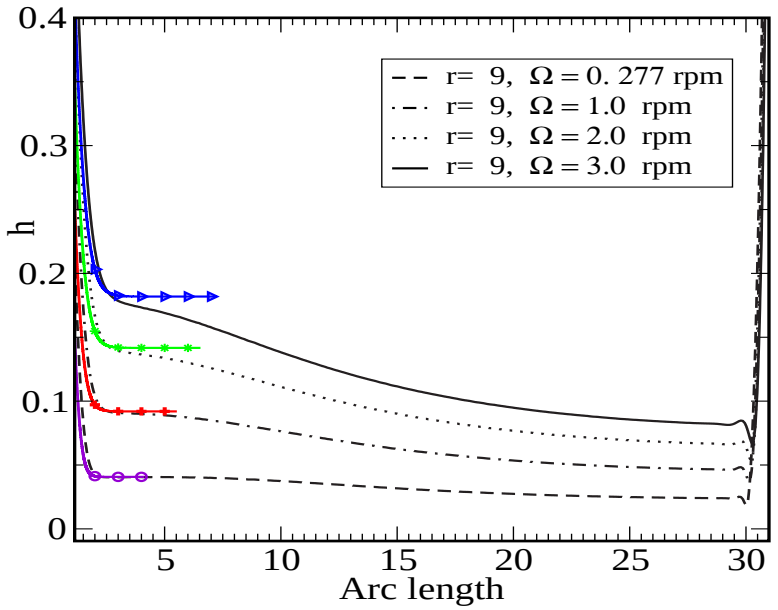

Figure 10: Meniscus profiles computed with the 1D model (4.84) (curves with symbols), for $\Omega = 0.277$ (circles), 1.0 (stars), 2.0 (plusses), 3.0 (triangles), and comparison with the profiles obtained for the cross section of the film profile for the rotating disk. "Arc length" denotes $r\theta$.

4.4 Comparison with the hyperbolic regime

Further out into the disk region the height profile will deviate from the height obtained for the Landau-Levich problem. There the variation of the height along the directions parallel to the disk is very small, which is clearly seen in our numerical simulations, so that surface tension will play a negligible role.

Starting from equation (2.41) we consider the steady state problem

$$\frac{\partial}{\partial r}\left[r\frac{h^3}{3}\sin\theta\right]+\frac{\partial}{\partial\theta}\left[\frac{h^3}{3}\cos\theta-\hat{\Omega}rh\right]=0, \tag{4.88}$$

to describe the dynamics far away from the meniscus. This can be simplified to the hyperbolic equation

$$h^2 r\sin\theta\frac{\partial h}{\partial r}+\left(h^2\cos\theta-\hat{\Omega}r\right)\frac{\partial h}{\partial\theta}=0\ . \tag{4.89}$$

Using the method of characteristics, this problem can be solved in form of an intitial value problem for the system of the coupled ordinary differential equations

$$\frac{dr}{d\tau} = h^2(r_0,0)\,r\sin\theta, \qquad r(0)=r_0\ , \tag{4.90a}$$

$$\frac{d\theta}{d\tau} = h^2(r_0,0)\cos\theta-\hat{\Omega}r, \qquad \theta(0)=0\ . \tag{4.90b}$$

Using as the initial condition the height found from (4.86) or simply by making use of formula (4.87) for a chosen r_0 we can integrate (4.90a), (4.90b) to obtain characteristics. This is shown in figure 11 for $\Omega = 0.277$ as an example. The results are similar for the other angular velocities. As can be seen, the comparison of the characteristics that start from the meniscus region shows good agreement with the contour lines found from the FEM computation. Note, that the contour lines that start at the boundary of the rotating disk strongly depend on the conditions there.

Interestingly, one can a good idea on the film profile as a function of the angular velocity $\hat{\Omega}$ by simply solving (4.90a), (4.90b) for r as a function of θ directly by taking

$$\frac{dr/d\tau}{d\theta/d\tau}=\frac{dr}{d\theta}=\frac{r\sin\theta}{\cos\theta-\hat{\Omega}r/h_0^2}\ , \tag{4.91}$$

which can be solved to yield

$$r(\theta)=\frac{h_0^2}{\hat{\Omega}}\left(\cos\theta\pm\sqrt{\cos^2\theta-2c_0\frac{\hat{\Omega}}{h_0^2}}\right), \tag{4.92}$$

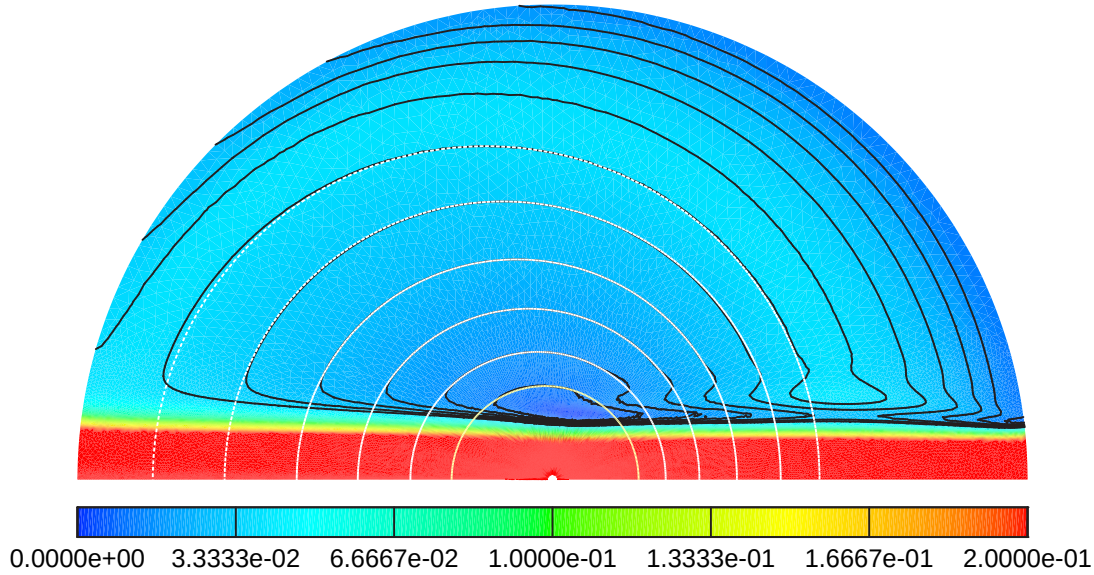

Figure 11: Comparison of contour lines from our FEM computation (black curves) for $\Omega = 0.277$ with the characteristics (white curves) for $r_0 = 1.962, 2.670, 3.560, 4.572, 5.759, 6.877$ and corresponding heights of $h_0 = 0.0130, 0.0182, 0.0234, 0.0286, 0.0338, 0.0390$, respectively. Note, the corresponding 3D plot in figure 6.

where the integration constant is

$$c_0 = r(0)\cos\theta(0) - \frac{\hat{\Omega} r^2(0)}{2h_0^2} \,. \tag{4.93}$$

5 Conclusions

In this work we set up a model for the fully three-dimensional free-boundary problem for the vertically rotating disk, drawing a thin film out of a liquid bath. We derived a dimension reduced generalized lubrication approximation. For this two-dimensional nonlinear degenerate fourth-order boundary value problem we developed a finite element scheme that captures the evolution of the film profile on the complete disk. For a range of parameters we found steady state solutions. Correspondingly, we performed an asymptotic analysis near the meniscus region and a careful comparison with cross sections of the numerical solutions along

constant radii gave excellent agreement. Moreover, we find that the height profile, even though dependent on the thickness that is determined by the meniscus region, can show considerable variations in the angular as well as the radial direction. We expect that these new steady state patterns will have implications for the application problem of a rotating disk in a PET-reactor. There, the chemical reaction depends crucially on the thickness of the thin film, see e.g. the article by Rafler et al. [14]. Our results will therefore give important information on the reaction rate to be expected for such a non-uniform film distribution.

It would be an interesting problem to also include visco-elastic effects into our model. This would also be more realistic when modelling highly viscous polymer films.

Acknowledgements

The authors acknowledge support by the DFG research center MATHEON, Berlin and the DFG grant WA 1626/1-1. AM also acknowledges support via the DFG grant MU 1626/3-1. We also gratefully acknowledge the help of Gerd Reinhardt with the visualization of the 3D plots.

References

[1] S. I. Cheong and K. Y. Choi. Melt polycondensation of polyethylene terephthalate in a rotating disk reactor. *J. Applied Polymer Sci.*, 58:1473–1483, 1995.

[2] M. S. Christodoulou, J. T. Turner, and S.D.R. Wilson. A model for the low to modererate speed performance of the rotating disk skimmer. *Journal of Fluids Engineering*, 112:476, 1990.

[3] R. A. Cook and R. H. Clark. An analysis of the stagnant band on falling liquid films. *Ind. Engng. Chem. Fundam.*, 12:106–114, 1973.

[4] T. A. Davis and I. S. Duff. An unsymmetric-pattern multifrontal method for sparse lu factorization. *SIAM J. Matrix Analysis and Applications*, 19: 140–158, 1997.

[5] A.G. Emslie, F.T. Bonner, and L.G. Peck. Flow of a viscous liquid on a rotating disk. *J. of Appl. Phys.*, 29:858–862, 1958.

[6] N. Fraysse and G.M. Homsy. An experimental study of rivulet instabilites in centrifugal spin coating of viscous newtonian and non-newtonian fluids. *Phys. Fluids*, 6:1491–1504, 1994.

[7] H.R.Schwarz. Methode der finiten elemente. Teubner Studienbücher, Stuttgart, 1991.

[8] H.S.Keshgi, S.F. Kistler, and L.E. Scriven. Rising and falling film flows: viewed from a first order approximation. *Chemical Engeneering Science*, 47: 683–694, 1992.

[9] Bioengineering Institute. Fem/bem notes. The Univeersity of Auckland, New Zealand, 2005.

[10] I. S. Kim, B. G. Woo, K. Y. Choi, and C. Kiang. Two-phase model for continuous final-stage melt polycondensation of polyethylene terephthalate. iii. modeling of multiple reactors with multiple reaction zones. *J. Applied Polymer Sci.*, 90:1088–1095, 2003.

[11] L. Landau and B. Levich. Dragging of a liquid by a moving plate. *Acta Physicochimica U.R.S.S.*, 17:42–54, 1942.

[12] A. Münch. The thickness of a Marangoni-driven thin liquid film emerging from a meniscus. *SIAM J. Appl. Math*, 62(6):2045–2063, 2002.

[13] T. G. Myers and J. P. F. Charpin. The effect of the coriolis force on axisymmetric rotating thin film flows. *International Journal of Non-Linear Mechanics*, 36:629–635, 2001.

[14] G. Rafler, E.G.R. Bonatz, and H. D. Otto. Zur kinetik der polykondensation von terephthalsäure und ethylenglykol in dünnen schmelzeschichten. *Acta Polymerica*, 38:6–10, 1979.

[15] R. Reinelt. Delaunay Gittergenerator. Technischer Bericht, Hermann-Föttinger-Institut, TU Berlin, 1995.

[16] B. Reisfeld, S. G. Bankoff, and S. H. Davis. The dynamics and stability of thin liquid films during spin coating. i. films with constant rates of evaporation or absorption. *J. Appl. Phys.*, 70:5258–5266, 1991.

[17] Th. Rieckmann and S. Völker. Pet polymerization - catalysis, reaktion mechanisms, kinetics, mass transport and reactor design. In J. Sheirs and T.E. Long, editors, *Modern Polyesters*. John Wiley & Sons, 2002.

[18] K. J. Ruschak. Flow of a falling film into a pool. *A. I. Ch. E. J.*, 24:705–709, 1978.

[19] S.D.R. Wilson. The drag-out problem in film coating theory. *J. Engg. Math.*, 16:209–221, 1982.

[20] S.D.R. Wilson and A.F. Jones. The entry of a falling film into a pool and the air-entrainment problem. *J. Fluid. Mech.*, 128:219–230, 1982.